Relating Fisher Information to Detectability of Changes in Nodule Characteristics with CT

Qin Li, Rongping Zeng, Kyle J. Myers, Berkman Sahiner, Marios A. Gavrielides, and Nicholas Petrick

Division of Imaging and Applied Mathematics, Office of Science and
Engineering Laboratories, Center for Devices and Radiological Health,
US Food and Drug Administration, Silver Spring, MD, USA

Abstract. Fisher information provides a bound on the variance of any unbiased estimate for estimation tasks involving nonrandom parameters. In addition, a Fisher information approximation for ideal-observer detectability has been derived. We adopt and generalize such an approximation to establish a method to assess a system's ability to detect small changes in lesion characteristics. By representing the lesion by a size parameter, the ability to detect small changes can be approximated by a function involving the size difference and the Fisher information. A concept, termed the approximated least required difference (ALRD), is introduced and evaluated as an upper bound for assessing a system's power in size discrimination. We present a simulation study for lung nodules as an example to illustrate such a framework, where the image model incorporates a simulated CT imaging system, a thorax background and parameterized nodules. The noise is assumed to be multivariate Gaussian and the noise power spectrum (NPS) method is used to estimate the covariance matrix for the Fisher information calculation. In addition to bounding performance, our results also provide insights into factors, including nodule characteristics and acquisition parameters, that influence ALRD performance. This framework can be extended to connect other discrimination and estimation tasks, facilitating objective assessment and optimization of quantitative imaging systems.

1 Introduction

Lung nodule growth or shrinkage is an important indicator of nodule malignancy, with growing nodules much more likely to be malignant. Likewise, tracking changes in nodule size as part of treatment monitoring allows patient response and treatment effectiveness to be monitored for individual patients. While early determination of small changes in nodules is desired, it is quite difficult due to the uncertainties associated with the imaging and size measurement processes. For instance, the standard RECIST criteria, which applies only for lesions of 10mm size or greater, only allows for determination of progressive disease when a 20% growth in longest diameter is observed [1]. There is a clear need for improved image acquisition and analysis methods that enable the detection of smaller changes in nodule size, and the quantification of such changes accurately, so they can be reliably applied to smaller nodules.

J.C. Gee et al. (Eds.): IPMI 2013, LNCS 7917, pp. 584–593, 2013.

Modern multi-detector row CT (MDCT) systems can now scan the whole lung within a single breath hold with a thin reconstructed slice thickness, facilitating 3D nodule volume estimation. However, efforts are still needed to quantitatively assess the bias and variance of volumetric measurements, which depend on a number of factors including scan acquisition and reconstruction parameters, nodule characteristics, and estimation methods [2]. In [3, 4], phantom studies were conducted to quantify the magnitude of such effects. Phantom studies provide a framework with known truth, enabling the determination of performance estimates under well-controlled conditions. It would also be useful to derive theoretical bounds on performance for this lung nodule volume estimation task and evaluate them by means of simulation studies, where we are not constrained to a limited set of nodule phantoms and imaging conditions.

Fisher information is a common construct in parameter estimation problems. It is well known that for estimation of nonrandom parameters, a lower bound of the variance of an unbiased estimator is given by the Cramer-Rao inequality, which is directly related to the Fisher information matrix. On the other hand, Fisher information also enters into the figure of merit for performance of classification tasks [5]. Intuitively, the performance of a classification task depends on how well the distributions of the classes are separated. Therefore, Fisher information must be tied with classification problems since it is also known as a metric to measure the informational difference between two probability distributions in information geometry [6].

The receiver operating characteristic (ROC) curve is a plot of the relationship between the true positive fraction and the false positive fraction for a decision-maker in a binary classification task, which is becoming increasingly widely used in the medical community [7]. Shen and Clarkson [8, 9] investigated the relation between Fisher information and area under the ROC curve (AUC), a figure of merit for binary classification problems. They derived a simple approximation relating the Fisher information to the detectability of a small change in the parameter of the probability distribution function (PDF) that governs the statistics of the data. In particular, the square of the detectability can be approximated to the second order as a product involving the parameter difference and the Fisher information.

Inspired by such a connection, we are proposing a method to assess the ability of a system to detect lesion size changes, particularly for the problem of lung nodule size change detection in CT images. Instead of looking at the signal size estimation task directly, we evaluate the difference that ensures size change detection at a certain level of detectability. By using the connection between Fisher information and AUC, we tie together estimation and detection tasks for this application.

2 Fisher Information and Detectability of Small Changes

We consider signals $\mathbf{f}(\mathbf{a})$ in physical space, parameterized by a nonrandom parameter vector $\mathbf{a}$. We denote the observed data as vector $\mathbf{g}$. For an estimation task, we wish to estimate parameter vector $\mathbf{a}$ from $\mathbf{g}$. Let $\hat{\mathbf{a}}(\mathbf{g})$ be an unbiased estimate, and ϵ_i be the ith component of the estimation error $\hat{\mathbf{a}}(\mathbf{g}) - \mathbf{a}$; then its variance satisfies

$$\sigma_{\epsilon_i}^2 \triangleq \mathrm{Var}\big(\, \hat{a}_i(\mathbf{g}) - a_i\big) \geq \big(F_{ii}(\mathbf{a})\big)^{-1} , \tag{1}$$

where the Fisher information matrix $\mathbf{F}(\mathbf{a}) = (F_{ij}(\mathbf{a}))$,

$$F_{ij}(\mathbf{a}) = \mathrm{E}\left\{\frac{\partial \ln pr(\mathbf{g}|\mathbf{a})}{\partial a_i} \cdot \frac{\partial \ln pr(\mathbf{g}|\mathbf{a})}{\partial a_j}\right\} , \tag{2}$$

assuming that the first and second derivative of $\ln pr(\mathbf{g}|\mathbf{a})$ exist [5], where $pr(\mathbf{g}|\mathbf{a})$ is the probability density of $\mathbf{g}$ conditioned on $\mathbf{a}$.

Instead of estimating $\mathbf{a}$, we are interested in detecting changes in $\mathbf{a}$. Assume there are two classes H_0 and H_1 of which the signal parameter vector has value $\mathbf{a}_0$ and $\mathbf{a}_1$ respectively. The question we address is determining which signal, $\mathbf{f}(\mathbf{a_0})$ or $\mathbf{f}(\mathbf{a_1})$, is present based on $\mathbf{g}$. The ideal-observer decides in favor of one or the other hypothesis by comparing the likelihood ratio Λ to a threshold, where

$$\Lambda = \frac{pr(\mathbf{g}|\mathrm{H}_1)}{pr(\mathbf{g}|\mathrm{H}_0)} \text{ , or alternatively, } \Lambda = \frac{pr(\mathbf{g}|\mathbf{a}_1)}{pr(\mathbf{g}|\mathbf{a}_0)} . \tag{3}$$

The ideal-observer utilizes all statistical information about the data, and as a result maximizes the AUC. Let $\Delta\mathbf{a} = \mathbf{a}_1 - \mathbf{a_0}$. Following [8, 9], we define $d_A(\mathbf{a}_0, \Delta\mathbf{a})$ as an index on the ability to differentiate between $\mathbf{f}(\mathbf{a}_0)$ and $\mathbf{f}(\mathbf{a}_1)$. The AUC and this index are related by

$$\mathrm{AUC} = \frac{1}{2} + \frac{1}{2}\mathrm{erf}\left(\frac{1}{2}\, d_A(\mathbf{a}_0, \Delta\mathbf{a})\right). \tag{4}$$

When $\Delta\mathbf{a}$ is small, by expanding $d_A^2(\mathbf{a_0}, \Delta\mathbf{a})$ at $\mathbf{a_0}$, a second order approximation is obtained as in [8]

$$d_A^2(\mathbf{a_0}, \Delta\mathbf{a}) \approx \Delta\mathbf{a}^T \cdot \mathbf{F}(\mathbf{a}_0) \cdot \Delta\mathbf{a} \ . \tag{5}$$

Hence, a firmer mathematical connection between the detection and estimation tasks is given by:

$$\mathrm{AUC} \approx \frac{1}{2} + \frac{1}{2}\mathrm{erf}\left(\frac{1}{2}\sqrt{\Delta\mathbf{a}^T \cdot \mathbf{F}(\mathbf{a}_0) \cdot \Delta\mathbf{a}}\right). \tag{6}$$

In [8], several examples for detecting weak signals were presented, showing high agreement between the approximation and the exact calculation of detection performance. In the remainder of this paper, we adopt and generalize this technique to our particular nodule size estimation task. To be more specific, we later introduce and evaluate ALRD, the approximated least required difference for differentiating spherical nodules of two different size estimates from reconstructed images. Compared to the formulation in previous studies where $\mathbf{f}(\cdot)$ was always linear in $\mathbf{a}$, $\mathbf{f}(\cdot)$ will be nonlinear in $\mathbf{a}$ in our work.

3 Image Model and Formulation of Fisher information

Let the imaging system be represented by

$$\mathbf{g}(\mathbf{x}; \mathbf{a}) = \mathcal{H} \circ \left(\mathbf{b}_{phy}(\mathbf{x}) + \mu\mathbf{f}(\mathbf{x}; \mathbf{a})\right) + \mathbf{n} \ , \tag{7}$$

where $\mathcal{H}$ represents a general imaging operator, linear or nonlinear, mapping the objects and background from physical space to image (reconstruction) space, $\mathbf{b}_{\text{phy}}(\mathbf{x}) \in \mathbb{R}^3$ is the background in physical space, $\mathbf{f}(\mathbf{x};\mathbf{a}) \in \mathbb{R}^3$ is the signal parameterized by a $m \times 1$ vector $\mathbf{a}$, μ is the density and $\mathbf{n}$ is the noise. Details of each component will be specified later. Let us emphasize that in the current formulation there are two sources of randomness in $\mathbf{g}$: the background and noise. For notational simplicity, we denote the noise-free image of the signal $\mathcal{H} \circ \mu\mathbf{f}(\mathbf{x};\mathbf{a})$ as $\mathbf{s}(\mathbf{a})$ and the noise-free image $\mathcal{H} \circ \left(\mathbf{b}_{\text{phy}}(\mathbf{x}) + \mu\mathbf{f}(\mathbf{x};\mathbf{a})\right)$ as $\bar{\mathbf{g}}$. Then the noise-free background image $\mathbf{b} \in \mathrm{B}$ is defined as $\mathbf{b} = \bar{\mathbf{g}} - \mathbf{s}(\mathbf{a})$. We further assume that $\mathbf{b}$ and $\mathbf{a}$ are independent. Now we derive the Fisher information at $\mathbf{a}_0$ by first manipulating $pr(\mathbf{g}|\mathbf{a})$. Let $\mathrm{L}(\mathbf{g}|\,\bar{\mathbf{g}}) = \ln pr(\mathbf{g}|\,\mathbf{b},\mathbf{a})$,

$$\begin{aligned}
\frac{\partial \ln pr(\mathbf{g}|\mathbf{a})}{\partial \mathbf{a}} &= \frac{1}{pr(\mathbf{g}|\mathbf{a})} \int_{\mathbf{B}} \frac{\partial pr(\mathbf{g}|\,\mathbf{b},\mathbf{a})}{\partial \mathbf{a}} pr(\mathbf{b})d\mathbf{b} \\
\text{(chain rule)} \quad &= \frac{1}{pr(\mathbf{g}|\mathbf{a})} \int_{\mathbf{B}} \frac{\partial pr(\mathbf{g}|\,\mathbf{b},\mathbf{a})}{\partial \mathbf{s}(\mathbf{a})} \frac{\partial \mathbf{s}(\mathbf{a})}{\partial \mathbf{a}} pr(\mathbf{b})d\mathbf{b} \\
&= \left(\int_{\mathbf{B}} \frac{\partial \ln pr(\mathbf{g}|\,\mathbf{b},\mathbf{a})}{\partial \mathbf{s}(\mathbf{a})} \frac{pr(\mathbf{g}|\,\mathbf{b},\mathbf{a}) pr(\mathbf{b})}{pr(\mathbf{g}|\mathbf{a})} d\mathbf{b} \right) \frac{\partial \mathbf{s}(\mathbf{a})}{\partial \mathbf{a}} \\
\text{(Byes's rule)} \quad &= \left(\int_{\mathbf{B}} \frac{\partial \mathrm{L}(\mathbf{g}|\,\bar{\mathbf{g}})}{\partial \mathbf{s}(\mathbf{a})} pr(\mathbf{b}|\mathbf{g},\mathbf{a})d\mathbf{b} \right) \frac{\partial \mathbf{s}(\mathbf{a})}{\partial \mathbf{a}} = \mathbf{G}(\mathbf{a}).
\end{aligned} \tag{8}$$

By definition, $\mathbf{F}(\mathbf{a}_0)$ is the mean of $\mathbf{G}(\mathbf{a}_0)^T\mathbf{G}(\mathbf{a}_0)$ over the ensemble of noisy $\mathbf{g}$ from class H_0, thus

$$\mathbf{F}(\mathbf{a}_0) = E\{\mathbf{G}(\mathbf{a}_0)^T\mathbf{G}(\mathbf{a}_0)\} \; . \tag{9}$$

Assume that the noise follows a multivariate Gaussian with zero mean and covariance matrix $\mathbf{K}$, then

$$pr(\mathbf{g}|\mathbf{b},\mathbf{a}) = \frac{1}{(2\pi)^{m/2}|\mathbf{K}|^{1/2}} exp\left(-\frac{1}{2}(\mathbf{g}-\bar{\mathbf{g}})^T\mathbf{K}^{-1}(\mathbf{g}-\bar{\mathbf{g}})\right) \tag{10}$$

and the derivative of the log likelihood function $\frac{\partial \mathrm{L}(\mathbf{g}|\bar{\mathbf{g}})}{\partial \mathbf{s}(\mathbf{a})} = (\mathbf{g}-\bar{\mathbf{g}})^T\mathbf{K}^{-1}$. Then $\mathbf{G}(\mathbf{a})$ becomes,

$$\mathbf{G}(\mathbf{a}) = \left(\mathbf{g} - \mathbf{s}(\mathbf{a}) - \int_{\mathbf{B}} \mathbf{b}pr(\mathbf{b}|\mathbf{g},\mathbf{a})\,\mathrm{d}\mathbf{b}\right)^{\mathrm{T}} \mathbf{K}^{-1} \left(\frac{\partial \mathbf{s}(\mathbf{a})}{\partial \mathbf{a}}\right) \tag{11}$$

If the $\mathbf{b}$ is fixed, according to the definition of $\mathbf{K}$,

$$\mathbf{F}(\mathbf{a}) = \left(\frac{\partial \mathbf{s}(\mathbf{a})}{\partial \mathbf{a}}\right)^T \mathbf{K}^{-1} \left(\frac{\partial \mathbf{s}(\mathbf{a})}{\partial \mathbf{a}}\right). \tag{12}$$

When $\mathbf{a}$ is a scalar, $\mathbf{F}(\mathbf{a})$ reduces to a scalar as well.

4 Simulations and Implementation

We simulated a helical multi-detector row CT scanner (MDCT). Our imaging operator $\mathcal{H}$ maps an object from the object space to the image space, including the forward projection and reconstruction process. The projection views of the virtual helical MDCT were generated by ray-tracing continuous objects that were analytically described by their parameters and then contaminated by the Poisson distribution. The reconstruction was obtained using the FBP-based helical CT image reconstruction algorithm [10]. Note that when the photo count I_0 is sufficiently large, the noise in the CT scans can be modeled reasonably well as a Gaussian distribution, ensured by the central limit theorem [11]. The reader may refer to [11] for more details about the MDCT simulation. The signal $\mathbf{f}(\mathbf{x};\mathbf{a})$ were modeled as location-known solid spheres parameterized by a single parameter, the diameter a.

Unlike some other medical images, such as mammography images, which feature a more complex textured background, the lung area background for a CT acquisition is relatively uniform when vessels and air pathway structures are not considered. Therefore, we have considered the background to be deterministic in this study. More realistic and complex backgrounds which increase the complexity of calculating the posterior mean in Eq. (11) will be studied in our future work. For now, we simulated a simplified thorax which contained large structures including the lung, heart, and spine (Fig.1a). The thorax, organs and other internal structures were modeled as analytical shapes, allowing the imaging process to be defined as a continuous-to-discrete mapping. The thorax (as illustrated in Fig. 1a) was modeled as an elliptical cylinder ($[r_x, r_y, l_z] = [17{,}10{,}35]\text{cm}, \mu = 40\text{HU}$); the two lungs were modeled as ellipsoids ($[r_x, r_y, r_z] = [7{,}5{,}15]\text{cm}, \mu = -850\text{HU}$); the heart was modeled as a sphere ($r = 3.5\text{cm}$, $\mu = 65\text{HU}$); the spine was modeled as two concentric cylinders ($[r_{out}, r_{in}, l_z] = [1.75{,}1.5{,}35]\text{cm}$, $[\mu_{out}, \mu_{in}] = [1000{,}200]\text{HU}$).

In general, the noise in CT is location dependent. However, within a small region, the noise properties vary slowly and can be viewed as locally stationary. Therefore, we used the noise power spectrum (NPS)-based approximation method to estimate the covariance matrix $\mathbf{K}$, operating under the assumption of stationary noise [12]. With the stationarity assumption, K can be diagonalized by the Fourier transform as $\mathbf{K} = \mathbf{A}^T\mathbf{W}\mathbf{A}$, where $\mathbf{A}$ is the Fourier transform matrix and $\mathbf{W}$ is a diagonal matrix, given by the NPS. The NPS can be empirically estimated by averaging the spectrum of the Fourier transforms of many realizations of noise. Since we were interested in small nodules, the NPS only needed to be calculated for a region of interest (ROI) around the nodule. In our simulations, the size of the ROI was chosen to be $15 \times 15 \times 7$ voxels around the nodule. For this ROI size, only around 30 noisy realizations were needed to produce a stable estimate of NPS [10]. Based on Eq. (14) and method of NPS, the Fisher information was then calculated as

$$F(a) = (\mathbf{A}\mathbf{s}'(a))^T\mathbf{W}^{-1}(\mathbf{A}\mathbf{s}'(a)) \,, \tag{13}$$

where $\mathbf{s}'(a)$ was numerically approximated using a finite difference technique since it was difficult to obtain an explicit expression for the first derivative of our signal.

Simulated images from the phantom and imaging model described above are shown in Fig.1. Fig.1a shows the central slice of the simple thorax with five 4mm (in diameter), -630HU spherical nodules centered at different locations within the xy-plane (all with the same z-direction position). Four are placed close to the boundary of the lung, in each of the four compass directions, and one in the center of the lung. The central slice of reconstruction passes through the nodule center. Note that although this image shows all five nodules, we only included a single nodule at one of these locations in the lung field for each realization to examine the location factor. We also included two cases where the nodules had the same xy-plane center as Location 1 but with a shift in z of 1mm (1/3 slice) and 1.5mm (1/2 slice), respectively. These situations were labeled as Location 6 and Location 7 (not shown in Fig.1a). The acquisition and reconstruction parameters were set as follows: $I_0 = 10^5$ (approximately equivalent to 100mAs), voxel size in x-, y- and z-dimensions were 0.78, 0.78 and 3mm respectively, targeted reconstruction ROI size was $15 \times 15 \times 7$ voxels around the nodule, reconstruction slice interval was 3mm with no overlap, the number of views was 300. Each NPS for a certain location was a $15 \times 15 \times 7$ matrix estimated from 30 noisy scans generated for each case. Fig. 1b shows images of the central slice of the 3D NPS for each location and Fig.1c shows the NPS for Location 2 as an example.

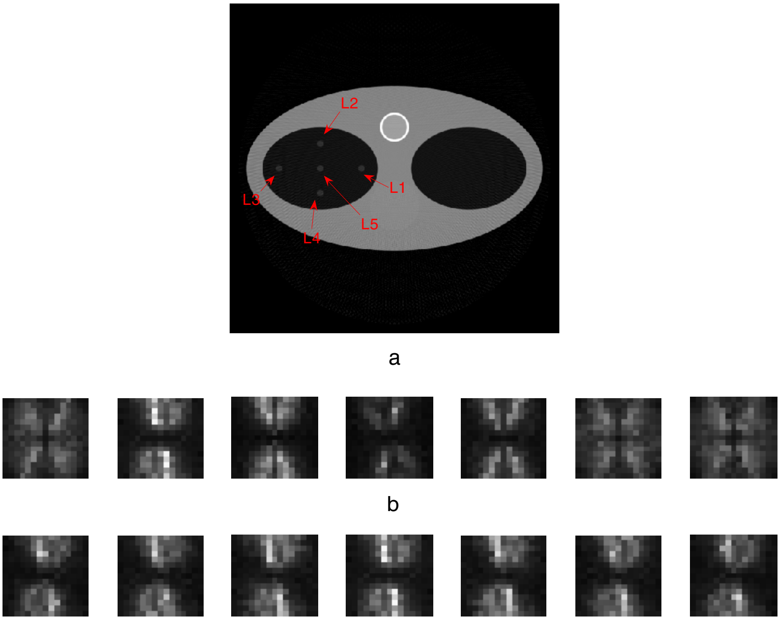

a

b

c

Fig. 1. a. Central slice of scan of the simplified thorax and nodule of Location 1-5. b. Examples of NPS (central slice) for the seven different nodule locations (Location 1-7 respectively). c. 3D NPS for a nodule centered at Location 2.

5 Approximated Least Required Difference (ARLD)

In practice, we often encounter the problem of determining whether or not a nodule size changes based on two estimates that are obtained at different time points without knowing the ground truth. To answer this question, we introduce the concept ALRD, the difference that ensures changes, at a given level of performance. First, let us define γ such that $|\Delta a| = \gamma a$. For a given nodule location l and γ, the approximated detectability is a function of a according to Eq. (5). We define the Fisher information approximation curve for a nodule at Location l as

$$C_l(\gamma; a) = \gamma a \sqrt{F(a)} \ . \tag{14}$$

Given l and γ, we assume that $C_l(\gamma; a)$ increases monotonically with a, i.e., the larger the nodule size is, the easier the detection of the same percentage for change. Therefore, there is a one-to-one relationship between any value of a and a particular C_l. For any desired level of detectability D for a change in nodule size, we can determine the associated nodule size parameter that gives that detectability value. We call the size parameter the critical size $a^\star_{\gamma,D}$ such that $C_l\left(\gamma; a^\star_{\gamma,D}\right) = D$. As we stated earlier, the detectability $d_A(a, \gamma a)$ (approximated by $C_l(\gamma, a)$) characterizes how well the ideal observer can differentiate nodules of size a and $(1 \pm \gamma)a$ after the objects are subjected to the imaging process. Thus, each D represents how well the distribution of the ideal observer test statistic for a nodule of size $a^\star_{\gamma,D}$ can be separated from that for a nodule of size $(1 \pm \mathrm{\gamma})a^\star_{\mathrm{\gamma,D}}$. The larger D is, the less likely an estimate $\hat{a} = (1+\gamma)a^\star_{\gamma,D}$ ($\hat{a} = (1-\gamma)a^\star_{\gamma,D}$) is from the distribution of nodules with ground truth size smaller (larger) than $a^\star_{\gamma,D}$. Let $\hat{a}_1, \hat{a}_2$ be two independent estimates with mean $a^\star_{\gamma,D}$. If $\hat{a}_1 > (1 + \frac{2\gamma}{1-\gamma})\hat{a}_2$ (equivalently, $\hat{a}_1 > (1+\gamma)a^\star_{\gamma,D}, \hat{a}_2 < (1-\gamma)a^\star_{\gamma,D}$), then we say their underlying truth has the relation $a_{true,1} > a_{true,2}$ with confidence level D and call $\rho(a^\star_{\gamma,D}) = \frac{2\gamma}{1-\gamma}$ the ARLD to tell a size change between nodules of two estimates around $\mathrm{a}^\star_{\mathrm{\gamma,D}}$ at confidence level D. ALRD by definition is then a function of baseline nodule size and certainty of belief. ARLD would be expected to hold not only for $a^\star_{\gamma,D}$ but for any $a > a^\star_{\gamma,D}$ because of the monotonicity of $C_l(\gamma; a)$. We suggest that $\mathrm{\rho}$ can be used as an overall figure of merit for assuring real change from size estimates for nodules that are subjected to an imaging process.

6 Results and Discussion

Fig. 2 shows the Fisher information approximation curves $C_l(\gamma; a)$ evaluated for $\gamma = 1\%$, Locations $l = 1,2,\ldots,7$ and $a = 3,4,\ldots,8mm$. For a fixed location, $C_l(\gamma; a)$ monotonically increases with increasing nodule diameter a, as we would expect. We see that $C_l(\gamma; a)$ varies with location, with nodule locations closer to more attenuating areas resulting in reduced detectability. We also observe that Locations 6 and 7, which are offset, also have impact on detectability. The right plot of Fig. 2 gives an example of $a^\star_{\gamma,D} = 5$ for Location 2, where $D = 4.35$ (or $\mathrm{AUC} = 0.999$) and $\gamma = 2.42\%$ ($\rho = 4.95\%$). This value of ALRD corresponds to roughly a 15% volume

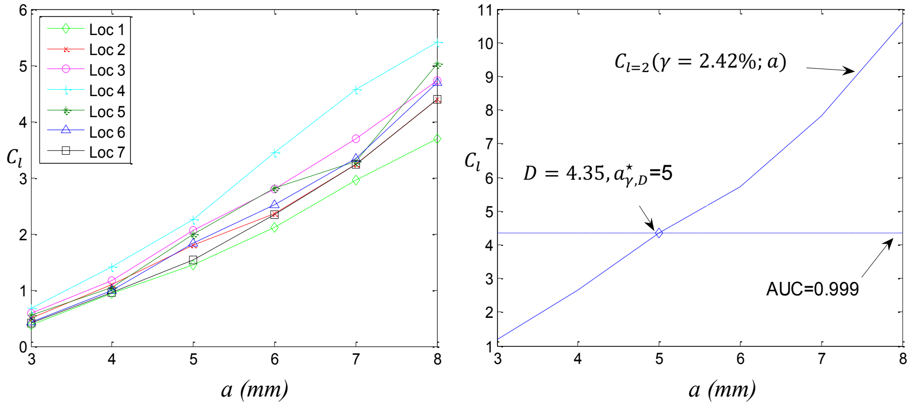

Fig. 2. Left: Plots of $C_l(1\%, a)$, the approximation to d_A, for locations $l = 1$ to 7. Right: Plot of $C_l(2.42\%, a)$ for Location 2 and the line $D = 4.35$ which corresponds to a 0.999 AUC. The intersection of these curves corresponds to a critical size of 5 mm.

difference in the spheres. Table 1 gives the ALRD for two *D* levels and different critical sizes, averaged among the seven locations. These results quantify the difficulty in determining the small changes in nodule size, especially for small nodules.

Table 1. ALRD (%) for different *D*(AUC) and critical sizes. Two quantities are given: the mean ALRD averaged across the seven locations and its standard deviation.

$a^\star_{\gamma,D}$ D	3mm	4mm	5mm	6mm	7mm	8mm
4.35 (0.999)	19.8 (4.56)	8.49 (1.20)	4.94 (0.81)	3.45 (0.54)	2.58 (0.34)	1.93 (0.24)
2.33 (0.95)	10.13 (2.23)	4.45 (0.62)	2.61 (0.42)	1.83 (0.29)	1.37 (0.18)	1.02 (0.13)

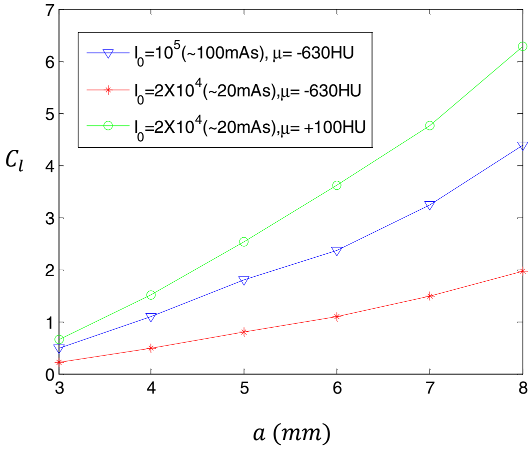

Fig. 3. Plots of curves $C_l(1\%, a)$ of Location 2 for three cases: (blue) -630HU nodule, $I_0 = 10^5$; (red) -630HU nodule, $I_0 = 2 \times 10^4$; (green) +100HU nodule, $I_0 = 2 \times 10^4$

Two more simulations were performed with a different simulated x-ray exposure I_0, one of which also involved a higher density object that resulted in higher contrast. Notice that the magnitude of the image of the object $\mathbf{s}(a)$, which is equal to $\mathcal{H} \circ \mu\mathbf{f}(\mathbf{x}; a)$, is directly proportional to μ. The NPS $\mathbf{W}$ for different doses (values of I_0) have similar shape but with magnitudes inversely proportional to I_0. Therefore, according to the formula for Fisher information (Eq. (13)), $\sqrt{F}$ should be directly proportional to μ and $\sqrt{I_0}$. Our numerical results given in Fig. 3 agree with this expectation: the d_A values of the blue curve are about $\sqrt{5}\times$ that of the red curve; the d_A values of the green curve are about $3\times$ that of the red curve (the attenuation coefficient of +100HU/-630HU is equivalent to $1.1\mu_{water}/0.37\mu_{water}$).

7 Conclusions and Future Work

In this work we establish a method to facilitate the quantitative assessment of imaging systems, especially by further relating detection tasks to estimation performance. To this point, we have provided insights into factors, including nodule characteristics (size and density) and acquisition parameters (dose and reconstruction slice center relative to nodule center), that influence ALRD performance. In particular, the results show that ALRD for detecting nodule change decreases when the true nodule size increases. ALRD was also found to be location dependent, and affected by factors such as CT dose and lesion contrast.

Questions remain regarding the quality of the approximations. The approximation formula was obtained by expanding d_A^2 by Taylor expansion. Therefore, the approximation is good when higher order terms have reasonable values [7]. Now consider the efficient estimator of a nonrandom parameter, i.e., one that is unbiased with a variance that achieves the Cramer-Rao lower bound. When an efficient estimator exists, this observer achieves maximal AUC. Assuming that the data $\mathbf{g}$ are normally distributed, one can show that the approximation is good as long as Δa is sufficiently small, and is exact when the signal is linear in a and the covariance matrices are the same for the two classes. In the situation where the parameter influences the data in a highly nonlinear manner, the Fisher information will not provide a tight bound for estimator performance.

In future work, we plan to explore the appropriateness of the approximations and especially how the derived bound compares with experimental results and how this work can be applied to clinical practice. The current formulation is general but the application here has some restrictions: the parameter is a scalar, and the background is deterministic. Thus, further studies are needed to evaluate the effectiveness of our method in more complicated problems (e.g., multi-parameter, random background). In addition, we plan to investigate the impact of additional CT imaging parameters, reconstruction algorithms, and complex nodules (irregular shape, mixed density) through the expansion of the model of the imaging process and the signals. The presented framework can be extended to connect other discrimination and estimation tasks as well. For instance, estimates of lesion shape features, such as sphericity, could be related to shape discrimination in a quantitative way. We hope this framework will eventually help facilitate objective assessment and optimization of quantitative imaging systems.

References

1. Eisenhauer, E.A., Therasse, P., Bogaerts, J., Schwartz, L.H., Sargent, D., Ford, R., Dancey, J., Arbuck, S., Gwyther, S., Mooney, M., Rubinstein, L., Shankar, L., Dodd, L., Kaplan, R., Lacombe, D., Verweij, J.: New response evaluation criteria in solid tumors: revised RECIST guideline (version 1.1). European Journal of Cancer 45(2), 228–247 (2009)
2. Gavrielides, M.A., Kinnard, L.M., Myers, K.J., Petrick, N.: Noncalcified lung nodules: Volumetric Assessment with thoracic CT. Radiology 251(1), 26–37 (2009)
3. Gavrielides, M.A., Zeng, R., Kinnard, L.M., Myers, K.J., Petrick, N.: Information-theoretic approach for analyzing bias and variance in lung nodule size estimation. IEEE Trans. on Med. Imag. 29, 1795–1807 (2010)
4. Gavrielides, M.A., Kinnard, L.M., Myers, K.J., Peregoy, J., Pritchard, W.F., Zeng, R., Esparza, J., Karanian, J., Petrick, N.: A resource for the assessment of lung nodule size estimation methods: database of thoracic CT scans of an anthropomorphic phantom. Optics Express 18, 15244–15255 (2010)
5. Van Trees, H.L.: Detection, Estimation, and Modulation Theory, Part I. Wiley (1968)
6. Amari, S.I.: Differential geometrical theory of statistics. Springer (1985)
7. Barret, H.H., Myers, K.J.: Foundations of Image Science. Wiley (2004)
8. Shen, F., Clarkson, E.: Using fisher information to approximate ideal-observer performance on detection tasks for lumpy-background images. JOSA A 23(10), 2406–2414 (2006)
9. Clarkson, E., Shen, F.: Fisher information and surrogate figures of merit for the task-based assessment of image quality. JOSA A 27(10), 2313–2326 (2010)
10. Hsieh, J.: Computed Tomography: Principles, Design, Artifacts and Recent Advances. SPIE Press, Bellingham (2003)
11. Zeng, R., Petrick, N., Gavrielides, M.A., Myers, K.J.: Approximations of noise covariance in multi-slice helical CT scans: impact on lung nodule size estimation. Med. Phys. 56, 6223–6242 (2011)
12. Siewerdsen, J.H., Cunningham, I.A., Jaffray, D.A.: A framework for noise-power spectrum analysis of multidimensional images. Med. Phys. 29, 2655–2671 (2002)